

This is the peer reviewed version of the following article: Li, X., Chen, Y., Wang, H., Yao, H., Huang, H., Mai, Y. W., ... & Zhou, L. (2016). Inserting Sn nanoparticles into the Pores of TiO<sub>2-x</sub>-C nanofibers by lithiation. *Advanced Functional Materials*, 26(3), 376-383, which has been published in final form at <https://doi.org/10.1002/adfm.201503711>. This article may be used for non-commercial purposes in accordance with Wiley Terms and Conditions for Use of Self-Archived Versions. This article may not be enhanced, enriched or otherwise transformed into a derivative work, without express permission from Wiley or by statutory rights under applicable legislation. Copyright notices must not be removed, obscured or modified. The article must be linked to Wiley's version of record on Wiley Online Library and any embedding, framing or otherwise making available the article or pages thereof by third parties from platforms, services and websites other than Wiley Online Library must be prohibited.

DOI: 10.1002/ ((please add manuscript number))

Article type: **(Full Paper)**

## Inserting Sn Nanoparticles into the Pores of TiO<sub>2-x</sub>-C Nanofibers by Lithiation

Xiaoyan Li,<sup>+</sup> Yuming Chen,<sup>+</sup> Hongtao Wang, Haimin Yao, Haitao Huang, Yiu-Wing Mai, Ning Hu and Limin Zhou\*

Dr. X.Y. Li,<sup>+</sup> Dr. Y.M. Chen,<sup>+</sup> Prof. H. M. Yao, Prof. Y. W. Mai, Prof. L. M. Zhou  
Department of Mechanical Engineering, The Hong Kong Polytechnic University, Hong Kong, China. Tel: 852-2766 6663; Fax: 852-2365 4703;  
E-mail: mmlmzhou@polyu.edu.hk

<sup>+</sup> The authors contributed equally.

Prof. H. T. Wang  
Institute of Applied Mechanics, Zhejiang University, Hangzhou, China.

Prof. H. T. Huang  
Department of Applied Physics and Materials Research Center, The Hong Kong Polytechnic University, Hong Kong, China.

Prof. Y. W. Mai  
Centre for Advanced Materials Technology (CAMT), School of Aerospace, Mechanical and Mechatronics Engineering J07, The University of Sydney, NSW 2006, Australia.

Prof. N. Hu  
College of Aerospace Engineering, Chongqing University, Chongqing, China.

**Keywords:** lithiation-induced insertion, TiO<sub>2-x</sub>-C-Sn hybrid nanofibers, *in situ* TEM, electrospinning, lithium ion batteries

Tin (Sn) holds promise as an anode material for lithium-ion batteries (LIBs) because of its high theoretical capacity, but its cycle life is limited by the structural degradation. Herein we exploited a novel approach to insert Sn nanoparticles into the pores of highly stable titanium dioxide-carbon (TiO<sub>2-x</sub>-C) nanofiber substrates that can effectively localize the post-formed smaller Sn nanoparticles and thereby address the problem of structural degradation and thus achieve improved performance. During first lithiation, Li<sub>4.4</sub>Sn alloy is inserted into the pores surrounding the initial Sn nanoparticles in TiO<sub>2-x</sub>-C nanofibers by its large volume expansion. Thereafter, the original Sn nanoparticle with diameter of about 150 nm cannot be recovered by the delithiation because of the surface absorption between inserted Sn nanoparticles and

the  $\text{TiO}_{2-x}\text{-C}$  substrate, resulting in many smaller Sn nanoparticles remained in the pores. Batteries containing these porous  $\text{TiO}_{2-x}\text{-C-Sn}$  nanofibers exhibit a high capacity of 957 mAh/g after 200 cycles at 0.1 A/g and can cycle over 10,000 times at 3 A/g while retaining 82.3 % of their capacity which represents the longest cycling life of Sn-based anodes for LIBs so far. This interesting method could provide new avenues for other high-capacity anode material systems that suffer from significant volume expansion.

## 1. Introduction

Rechargeable LIBs are regarded as a promising power source for electronic devices such as electric vehicles and hybrid electric vehicles.<sup>[1-5]</sup> Graphite, as the most intensely used commercial anode material, has a low theoretical capacity of 372 mAh/g, which makes it difficult to meet the demanding for high energy density in energy storage systems. Recently, Sn has been widely studied as an anode material for LIBs due to its high theoretical capacity of 991 mAh/g. However, the rapid fading of capacity that results from the great change in volume during the alloying-dealloying reaction between Sn and Li renders the achievement of a long cycle life difficult.<sup>[6-12]</sup> Recent years, great efforts have been devoted to solve the above issues by (a) engineering nanostructure to reduce the volume expansion; (b) incorporating Sn with other phases, including carbon and titanium dioxide ( $\text{TiO}_2$ ), not only to prevent the aggregation of Sn but serve as buffer scaffold.<sup>[13-23]</sup> Nevertheless, long-term cycling performance of the existing Sn-based anode remains unsatisfactory. To obtain desirable cycling performance, our objective is to scrupulously design a robust porous one-dimensional (1D)  $\text{TiO}_{2-x}\text{-carbon}$  ( $\text{TiO}_{2-x}\text{-C}$ ) substrate to encapsulate Sn nanoparticles, in which the firm  $\text{TiO}_{2-x}\text{-C}$  substrate can fully absorb the volume expansion of the Sn nanoparticles in the  $\text{TiO}_{2-x}\text{-C}$  substrate during charging-discharging processes (which can be directly observed by *in situ* transmission electron microscopy [TEM]) and thus achieve a long life.

In this study, for the first time, we present a novel approach of lithiation-induced insertion of Sn nanoparticles into the pores of the highly stable  $\text{TiO}_{2-x}\text{-C}$  nanofiber substrates, which

can effectively localize the Sn nanoparticles and allow superior performance. *In situ* TEM was performed to characterize the structural evolution of the prepared material during the charging and discharging processes. It was found that  $\text{Li}_{4.4}\text{Sn}$  alloy was inserted into the pores surrounding the initial Sn nanoparticles in the  $\text{TiO}_{2-x}\text{-C}$  nanofibers by its large volume expansion. The initial Sn nanoparticle with diameter of about 150 nm could not be recovered after discharging due to the surface absorption between smaller separated Sn nanoparticles and  $\text{TiO}_{2-x}\text{-C}$  substrate. These detached Sn nanoparticles remained in the pores which are able to accommodate their expansions, thus yielding a very long cycle life.

## 2. Introduction

### 2.1 Synthesis and characterization of highly stable porous $\text{TiO}_{2-x}\text{-C-Sn}$ composite nanofibers.

The detailed fabrication process is shown in **Figure 1**. First, the  $\text{Ti}(\text{OiPr})_4$ -polystyrene-tin(II)2-ethylhexanoate fibers were synthesized through simple electrospinning. The electrospun  $\text{Ti}(\text{OiPr})_4$ -polystyrene-tin(II)2-ethylhexanoate fibers were treated at 450 °C in an atmosphere of  $\text{N}_2$  to obtain porous  $\text{TiO}_2\text{-C-SnO}_x$ , in which part of the polystyrene turned into carbon and others were burnt out to form pores, followed by treatment in a mixture of  $\text{C}_2\text{H}_2/\text{H}_2/\text{Ar}$  at 700 °C to achieve porous  $\text{TiO}_{2-x}\text{-C-Sn}$  composite nanofibers. Some parts of the  $\text{Ti}^{4+}$  were reduced to  $\text{Ti}^{3+}$  by heating in a hydrogen atmosphere, which resulted in the presence of oxygen vacancies and  $\text{Ti}^{3+}$  species and thus effectively improved the electrical conductivity of  $\text{TiO}_2$ .<sup>[24-26]</sup>

The FESEM and TEM images in **Figure 2a, b** reveal the fibrous morphology of the resulting materials, with a highly porous surface of nanofibers with diameters of 400 to 500 nm. These surface pores facilitate rapid access of the lithium ions into the inner fibers, yielding a good rate capability and activation of all of the materials. It is clear that the Sn nanoparticles are encapsulated in the porous  $\text{TiO}_{2-x}\text{-C}$  composite substrate as shown in Figure

2c, d. A magnified image in Figure 2e exhibits the highly porous inner structure, which is beneficial for accommodation of the variation in the volume of Sn during repeated charging and discharging cycles. The prepared  $\text{TiO}_{2-x}\text{-C-Sn}$  hybrid shows a relatively high Brunauer-Emmett-Teller specific area of  $83.1 \text{ m}^2 \text{ g}^{-1}$  with a pore volume of  $0.285 \text{ cm}^3 \text{ g}^{-1}$ . As shown in Figure S1a, the pore size distribution curve calculated by a non-local density functional theory method indicates that the prepared hybrid involves nanopores ranging in size from 1.5 to 68 nm. Figure S1b shows the isothermal plot of the porous  $\text{TiO}_{2-x}\text{-C-Sn}$  composite nanofibers, which is characteristic of the porous structure.<sup>[27]</sup> The high-resolution TEM image in Figure 2f confirms the presence of tetragonal Sn ( $d_{\text{Sn}(200)} = 0.29 \text{ nm}$ ), rutile  $\text{TiO}_2$  ( $d_{\text{TiO}_2(101)} = 0.24 \text{ nm}$ ), and carbon, which is consistent with the results of **selected area electron diffraction (SAED, Figure 2d)**, XRD (**Figure 3a**) and Raman analysis (Figure S2).<sup>[9,28]</sup>

The surface chemistry of the porous  $\text{TiO}_{2-x}\text{-C-Sn}$  composite nanofibers was analyzed by XPS. The typical XPS spectrum of  $\text{TiO}_{2-x}\text{-C-Sn}$  nanofibers in Figure S3a demonstrates the existence of C, Ti, Sn, and O, which is in good agreement with the result of EDS in Figure S4 and the elemental line scanning in Figure S5. As shown in Figure 3b, the Sn 3d spectrum displays two typical peaks at 487.2 and 495.7 eV, assigning to Sn 3d<sub>5/2</sub> and Sn 3d<sub>3/2</sub>, which shows that some Sn nanoparticles near the surface of the fiber have been oxidized into  $\text{SnO}_2$ .<sup>14,29,30</sup> Peak separation of the Ti 2P spectrum in Figure 3c presents four peaks with binding energies of 458, 463.5, 458.7, and 464.5 eV, respectively. The peaks at 458 and 463.5 eV are attributed to  $\text{Ti}^{3+}$ , and the bands at 458.7 and 464.5 eV are attributed to  $\text{Ti}^{4+}$ .<sup>31,32</sup> The composition distribution in Table S1 demonstrates the existence of nonstoichiometric titanium suboxides. The high-resolution XPS spectrum of C 1s (Figure 3d) can be deconvoluted into three peaks. The peak at 284.5 eV is assigned to the C-C bonds, and the other two peaks at 285.8 and 288 eV correspond to the C-O and C=O bonds, **which would be due to the partial substitution of some of lattice titanium atoms by carbons and the organic carbonaceous**

material resulting from the calcination of oxygen-containing organic precursors such as tin(II)2-ethylhexanoate, respectively.<sup>16,32-35</sup> In Fig. S3b, the O 1s spectrum is divided into three peaks at 530 eV (Ti-O), 531 eV (H-O), and 532.5 eV (C-O).<sup>16</sup>

## 2.2 Morphology evaluation of the TiO<sub>2-x</sub>-C-Sn composite nanofibers upon cycling.

*In situ* TEM was used to observe the structural evolution of the prepared material during the processes of charging and discharging. **Figure 4** shows the typical morphological evolution of Sn nanoparticles encapsulated in the porous TiO<sub>2-x</sub>-C nanofiber during the first five charging and discharging processes. Obvious volume expansion occurred after the first lithiation, as shown in Figure 4a. Apparently, the pores surrounding the Sn nanoparticles in the composite nanofiber were able to absorb the expansion of the Sn nanoparticles without inducing a change in the volume of the TiO<sub>2-x</sub>-C composite nanofiber substrate, proving the firmness and excellent mechanical properties of TiO<sub>2-x</sub>-C matrix. The uniform dark contrast of Sn nanoparticles became lighter with the reaction processing. The Sn nanoparticles underwent a volume change of approximately 260 % at the completion of the first charging process. The lithium was gradually extracted from the Li-Sn alloys when the process of delithiation began, as displayed in Figure 4b. The Sn nanoparticles separated into smaller particles after the first discharging process due to the surface absorption force between Sn nanoparticle and TiO<sub>2-x</sub>-C substrate.<sup>[36]</sup> The separated Sn nanoparticles did not recover their original volume after the second lithiation (Figure 4c). The smaller Sn nanoparticles remained in the pores toward which the initial Sn nanoparticles expanded. These pores were able to accommodate the expansion of the separated Sn nanoparticles with diameter ranging from 2 nm to 30 nm, which can be shown by the lack of a clear change in Figure 4d as compared with Figure 4c.

*Ex situ* TEM was also used to observe the structural changes in the porous TiO<sub>2-x</sub>-C-Sn nanofibers after different charge-discharge cycles (**Figure 5**). The Sn nanoparticles, which occupy the pores that surround them, are unable to convert back to their original state after the

first charge-discharge cycle. The enlarged figure inset in Figure 5a and line scanning in Figure 5b confirm the detachment of the Sn nanoparticles into smaller particles. Obviously, the size of the Sn nanoparticles decreased greatly as induced by lithiation after 1000 cycles, as shown in Figure 5c. The line scanning in Figure 5d demonstrates the uniform distribution of the smaller Sn nanoparticles in the porous  $\text{TiO}_{2-x}\text{-C}$  substrate, facilitating the transport of electrons, which can be proven by the electrochemical impedance spectroscopy shown in Figure S6. The high-resolution TEM images in the insets of Figure 5a and 5c clearly demonstrate that the crystalline structure of Sn and  $\text{TiO}_2$  does not change after cycling. In addition, no loss of Sn can be found, which demonstrates great stability.

### 2.3 Electrochemical performance

The electrochemical performance of the  $\text{TiO}_{2-x}\text{-C-Sn}$  electrode is evaluated in **Figure 6**. Figure 6a depicts the charge-discharge voltage profiles of the  $\text{TiO}_{2-x}\text{-C-Sn}$  nanofibers at a current density of 0.1 A/g. The discharge and charge capacities are 1562 and 1045 mAh/g, respectively, displaying a Coulombic efficiency of 67 %. The loss of capacity can be ascribed to the formation of an solid electrolyte interface layer and the decomposition of electrolytes.<sup>[9,13,14,37,38]</sup> It is worth noting that the correlative plateaus are in good agreement with the cyclic voltammetry results in Figure S7.<sup>6,10,39,40</sup> Figure 6b compares the cycling performance of three electrodes made of  $\text{TiO}_{2-x}\text{-C-Sn}$ ,  $\text{TiO}_2\text{-C}$ , and  $\text{TiO}_2$  nanofibers at a current density of 0.1 A/g between 0 and 3 V. The capacity of  $\text{TiO}_{2-x}\text{-C-Sn}$  nanofibers decreases during the first few cycles and then gradually rises, finally reaching and maintaining 957 mA h/g after 200 cycles. The increase in capacity is mainly a result of the material activation after cycling. In comparison, the  $\text{TiO}_2\text{-C}$  and  $\text{TiO}_2$  electrodes can only deliver capacities of 422 mAh/g and 122 mAh/g at 0.1 A/g, respectively. The  $\text{TiO}_{2-x}\text{-C-Sn}$  electrode was assessed by charging and discharging at different rates from 0.5 to 5 A/g, as shown in Figure 6c. It maintains high reversible capacities of 374, 336, 275, 204, and 133

mAh/g at 0.5, 1, 2, 3, and 5 A/g, respectively, and the capacity of 275 mAh/g can be attained again when the current density returns to 2 A/g. Most importantly, the battery can cycle over 10000 times with a remained capacity of 140 mAh/g at 3 A/g (Figure 6c), which kept more than 82.3 % of their capacity (0.177 % decay per 100 cycles), showing a very long cycling life. While the capacity of TiO<sub>2</sub> only remains at 40 mAh/g at 3 A/g, as shown in Figure S8. To the best of our knowledge, this is the longest cycling life of Sn-based anodes which has not discovered before. Figure S9 shows the charge-discharge profiles after 200 cycles and at different current densities. It is clear that the the plateaus of Sn lithiation and delithiation can be obviously observed after 200 cycles (Figure S9a), indicating that the Sn nanomaterials are still well maintained in the TiO<sub>2-x</sub>-C composite substrate. Furthermore, the contributions of different components to the whole capacity can also be seen through these charge-discharge profiles. The measurement on electrochemical performance of the hybrid materials in the voltage range of 0-1 V has been also conducted (Figure S10). Figure S10a shows that the porous TiO<sub>2-x</sub>-C-Sn nanofibers have the reversible capacity of ~ 443 mAh g<sup>-1</sup> after 10 cycles at 0.1 A/g based on the mass of the whole composite. If based on the mass of Sn (48.12 wt.% of Sn in the composite, Table S1), the reversible capacity can be up to 920 mAh g<sup>-1</sup>, which is close to the theoretical capacity of Sn. Moreover, this hybrid material still has high capacities of ~ 622, 538, 500, 408 and 311 mAh g<sup>-1</sup> at current densities of 0.4, 0.6, 0.8, 1, and 2 A g<sup>-1</sup>, respectively, based on the mass of Sn. These results show that our material possesses high electrochemical performance. For the practical application, the low Coulombic efficiency for the composite in the inial cycle would be addressed by creating a passivation layer on the surface of the prepared anode.<sup>3</sup> The superior electrochemical performance of the TiO<sub>2-x</sub>-C-Sn nanofibers may be attributable to the following benefits. i) The high theoretical capacity of Sn contributes to the capacity of the nanofiber substrate. ii) The TiO<sub>2-x</sub> nanofiber substrate leads to structural stability and thus to good cyclability. iii) The porous structure provides void space to accommodate the changes in volume of Sn nanoparticles during the charging and

discharging cycles, which is beneficial for maintaining the integrity of the material and further enhancing the cycle life. iv) 1D nanostructure and carbon facilitate the rapid transport of ion and electrons and yield an excellent rate capability.<sup>41,42</sup> v) Ti<sup>3+</sup>-doped TiO<sub>2-x</sub> results in a significant increase in electronic conductivity, which benefits electrochemical lithium storage.

### 3. Conclusions

In summary, we exploited a novel approach of lithiation-induced insertion of Sn nanoparticles into the pores of highly stable TiO<sub>2-x</sub>-C nanofiber substrates to address the problem of structural degradation of Sn-based electrode. The *in situ* TEM observation has proved that during first lithiation Li<sub>4.4</sub>Sn alloy can be effectively inserted into the pores surrounding the initial Sn nanoparticles in the TiO<sub>2-x</sub>-C nanofibers by its large volume expansion and after first delithiation the post-formed smaller Sn nanoparticles remain in the pores. Benefiting from the unique structural and compositional features, the as-made TiO<sub>2-x</sub>-C-Sn nanofibers as anode have achieved a long cycling life of over 10000 charging/discharging cycles in addition to a high specific capacity of 957 mAh/g at 0.1 A/g and good rate capability. We believe that this novel and simple approach could provide new avenues for synthesizing other high-performance anode material systems that suffer from large volume expansion.

### 4. Experimental Section

#### *Synthesis of 1D porous TiO<sub>2-x</sub>-C-Sn composite nanofibers*

A 3 g sample of polystyrene (M<sub>w</sub> ~280 000) was dissolved in 20 mL of dimethylformamide at 70 °C for 5 h with vigorous stirring. Then, 1 mL of acetic acid and 3 mL of Ti(OiPr)<sub>4</sub> were added dropwise into the polystyrene solution, followed by 1 mL of tin(II)2-ethylhexanoate. The precursor solution was used for electrospinning at a high voltage of 17 kV. The distance between the needle and the drum collector was fixed at 20 cm, and the feeding rate was set at 0.04 mm/min (KATO Tech Co., Ltd). The collected films were first heated at 450 °C in an atmosphere of N<sub>2</sub> and then treated in a C<sub>2</sub>H<sub>2</sub>/H<sub>2</sub>/Ar mixture at 700 °C for 30 min to prepare porous TiO<sub>2-x</sub>-C-Sn



composite nanofibers.

#### *Characterization*

The morphologic features of the samples were examined by field emission scanning electron microscopy (FESEM, JEOL 6300F), TEM, and high-resolution TEM (JEOL 2100F). A JEOL 2100 TEM equipped with a Nanofactory STM-TEM holder was used to conduct the *in-situ* electrochemical experiments. The crystal structure was examined by x-ray diffraction (XRD, Philips X'Pert Pro MPD). Measurement by x-ray photoelectron spectroscopy (XPS) was performed on a Perkin-Elmer model PHI 5600 system with a monochromated aluminum anode x-ray source. A Micromeritics ASAP2020 analyzer was used to evaluate the surface area.

#### *Electrochemical test*

The electrochemical performance of the  $\text{TiO}_{2-x}\text{-C-Sn}$  composite nanofiber electrode was measured using CR 2032 coin cells that were assembled in an Ar-filled glove box. The working electrode was made of the active materials, carbon black and polyvinylidene fluoride binder slurry in a weight ratio of 8:1:1, which was coated on the copper foil current collector. Metallic lithium was used as the counter electrode, and celgard 2400 film was used as the separator. The electrolyte solution was 1M of  $\text{LiPF}_6$  in a mixture of ethylene carbonate/diethyl carbonate (1:1 v/v). The charge and discharge tests were carried out in the range of 0 to 3 V with a battery testing system (LAND 2001 CT). Cyclic voltammetry was performed on a CHI 660C electrochemical workstation between 0 and 3 V at a scan rate of  $0.1 \text{ mV s}^{-1}$ .

#### **Supporting Information**

Supporting Information is available from the Wiley Online Library or from the author.

#### **Acknowledgements**

The authors are grateful for the support received from the Research Grants Council of the Hong Kong Special Administration Region (grants: PolyU5312/12E) and the Hong Kong Polytechnic University (grants: G-YBA1, G-YBDG, 1-BBZN).

Received: ((will be filled in by the editorial staff))

Revised: ((will be filled in by the editorial staff))

Published online: ((will be filled in by the editorial staff))

- [1] Y. Guo, L. Yu, C. Y. Wang, Z. Lin and X. W. Lou, *Adv. Funct. Mater.* **2015**, 25, 5184.
- [2] B. Zhang, J. Q. Huang and J. K. Kim, *Adv. Funct. Mater.* **2015**, 25, 5222.
- [3] Y. M. Chen, X. Y. Li, K. Park, J. Song, J. H. Hong, L. M. Zhou, Y. W. Mai, H. T. Huang and J. B. Goodenough, *J. Am. Chem. Soc.* **2013**, 135, 16280.
- [4] H. Hu, L. Yu, X. H. Gao, Z. Lin and X. W. Lou, *Energy Environ. Sci.* **2015**, 8, 1480.
- [5] L. Zhang, H. B. Wu, B. Liu and X. W. Lou, *Energy Environ. Sci.* **2014**, 7, 1013.
- [6] W. M. Zhang, J. S. Hu, Y. G. Guo, S. F. Zheng, L. S. Zhong, W. G. Song and L. J. Wan, *Adv. Mater.* **2008**, 20, 1160.
- [7] Y. Yu, G. Lin, C. L. Wang, A. Dhanabalan, P. A. V. Aken and J. Maier, *Angew. Chem. Int. Ed.* **2009**, 48, 6485.
- [8] Y. H. Xu, Q. Liu, Y. J. Zhu, Y. H. Liu, A. Langrock, M. R. Zachariah and C. S. Wang, *Nano Lett.* **2013**, 13, 470.
- [9] Y. Q. Zou and Y. Wang, *ACS Nano* **2011**, 5, 8108.
- [10] Y. Yu, L. Gu, C. B. Zhu, P. A. V. Aken and J. Maier, *J. Am. Chem. Soc.* **2009**, 131, 15984.
- [11] Z. Q. Zhu, S. W. Wang, J. Du, Q. Jin, T. R. Zhang, F. Y. Cheng and J. Chen, *Nano Lett.* **2014**, 14, 153.
- [12] Z. H. Wen, S. M. Cui, H. Kim, S. Mao, K. Yu, G. H. Lu, H. H. Pu, O. Mao and J. H. Chen, *J. Mater. Chem.* **2012**, 22, 3300.
- [13] D. Deng and J. Y. Lee, *J. Mater. Chem.* **2010**, 20, 8045.
- [14] J. Qin, C. N. He, N. Q. Zhao, Z. Y. Wang, C. S. Shi, E. Z. Liu and J. J. Li, *ACS Nano* **2014**, 8, 1728.

- [15] G. H. Zhang, J. Zhu, W. Zeng, S. C. Hou, F. L. Gong, F. Li, C. C. Li and H. G. Duan, *Nano Energy* **2014**, 9, 61.
- [16] X. Y. Li, Y. M. Chen, L. M. Zhou, Y. W. Mai and H. T. Huang, *J. Mater. Chem. A*, **2014**, **2**, 3875.
- [17] X. Y. Li, Y. M. Chen, H. M. Yao, X. Y. Zhou, J. Yang, H. T. Huang, Y. W. Mai and L. M. Zhou, *RSC Adv.* **2014**, 4, 39906.
- [18] Y. X. Tang, Y. Y. Zhang, J. Y. Deng, J. Q. Wei, H. L. Tam, B. K. Chandran, Z. L. Dong, Z. Chen and X. D. Chen, *Adv. Mater.* **2014**, 26, 6111.
- [19] H. G. Wang, D. L. Ma, X. L. Huang, Y. Huang and X. B. Zhang, *Sci. Rep.* **2012**, 2, 701.
- [20] G. Q. Zhang, H. B. Wu, T. Song, U. Paik and X. W. Lou, *Angew. Chem. Int. Ed.* **2014**, 53, 1.
- [21] Y. Y. Zhou, C. S. Jo, J. Lee, C. W. Lee, G. J. Qao and S. H. Yoon, *Micropor. Mesopor. Mat.* **2012**, 151, 172.
- [22] J. Z. Chen, L. Yang, Z. X. Zhang, S. H. Fang and S. I. Hirano. *Chem. Commun.* **2013**, 49, 2792.
- [23] J. Y. Liao and A. Manthiram, *Adv. Energy Mater.* **2014**, 4, 1400403.
- [24] J. Y. Shin, J. H. Joo, D. Samuelis and J. Maier, *Chem. Mater.* **2011**, 24, 543.
- [25] X. Lu, G. Wang, T. Zhai, M. Yu, J. Gan, Y. Tong and Y. Li, *Nano Lett.* **2012**, 12, 1690.
- [26] M. Stefik, F. J. Heiligttag, M. Niederberger and M. Grätzel, *ACS Nano* **2013**, 7, 8981.
- [27] M. Kruk and M. Jaroniec, *Chem. Mater.* **2001**, 13, 3169.
- [28] J. H. Jeun, K. Y. Park, D. H. Kim, W. S. Kim, H. C. Kim, B. S. Lee, H. G. Kim, W. R. Yu, K. Kang and S. H. Hong, *Nanoscale* **2013**, 5, 8480.
- [29] L. Wang, D. Wang, Z. H. Dong, F. X. Zhang and J. Jin, *Nano Lett.* **2013**, 13, 1711.
- [30] B. Zhang, Q. B. Zheng, Z. Huang, S. W. Oh and J. K. Kim, *Carbon* **2011**, 49, 4524.
- [31] X. Liu, H. Xu, L. R. Grabstanowicz, S. M. Gao, Z. Z. Lou, W. J. Wang, B. B. Huang, Y. Dai and T. Xu, *Catal. Today* **2014**, 225, 80.

- [32] Z. Liang, G. Zheng, W. Li, Z. W. Seh, H. Yao, K. Yan, D. Kong and Y. Cui, *ACS Nano* **2014**, 8, 5249.
- [33] L. Zhang and G. Q. Shi, *J. Phys. Chem. C* **2011**, 115, 17206.
- [34] T. Xu, W. Hou, X. Shen, H. Wu, X. Li, J. Wang and Z. Jiang, *J. Power Sources* **2011**, 196, 4934.
- [35] J. D. Zhuang, Q. F. Tian, H. Zhou, Q. Liu, P. Liu and H. M. Zhong, *J. Mater. Chem.* **2012**, 22, 7036.
- [36] X. R. Xia, N. A. Monteiro-Riviere, S. Mathur, X. F. Song, L.S. Xiao, S. J. Oldenberg, B. Fadeel and J. E. Riviere, *ACS Nano* **2011**, 5, 9074.
- [37] L. Qie, W. M. Chen, Z. H. Wang, Q. G. Shao, X. Li, L. X. Yuan, X. L. Hu, W. X. Zhang and Y. H. Huang, *Adv. Mater.* **2012**, 24, 2047.
- [38] B. Zhang, Y. Yu, Z. D. Huang, Y. B. He, D. H. Jang, W. S. Yoon, Y. W. Mai, F. Y. Kang and J. K. Kim, *Energy Environ. Sci.* **2012**, 5, 9895.
- [39] S. Q. Chen, P. Chen, M. H. Wu, D. Y. Pan and Y. Wang, *Electrochem. Commun.* **2010**, 12, 1302.
- [40] S. Q. Chen, Y. Wang, H. J. Ahn and G. X. Wang, *J. Power Sources* **2012**, 216, 22.
- [41] Y. M. Chen, X. Y. Li, X. Y. Zhou, H. M. Yao, H. T. Huang, Y. W. Mai and L. M. Zhou, *Energy Environ. Sci.* **2014**, 7, 2689.
- [42] Y. M. Chen, Z. G. Lu, L. M. Zhou, Y. W. Mai and H. T. Huang, *Nanoscale* **2012**, 4, 6800.



**Figure 1.** Schematic illustration of the formation of highly stable porous  $\text{TiO}_{2-x}\text{-C-Sn}$  composite nanofibers and insertion of Sn nanoparticles.

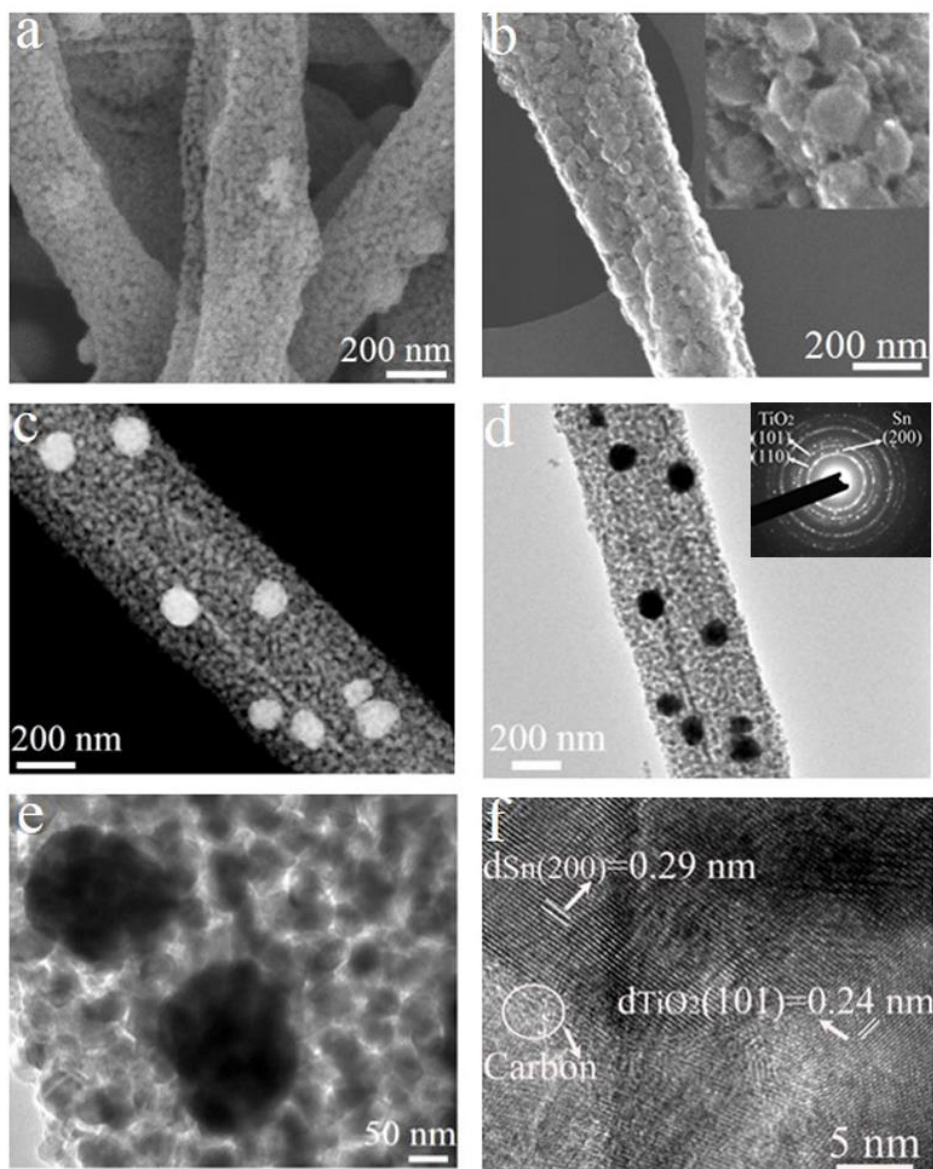


**Figure 2.** Morphology of the highly stable porous  $\text{TiO}_{2-x}\text{-C-Sn}$  composite nanofibers. (a) FESEM, (b) TEM-SEI, (c) TEM-BF, (d) and (e) TEM, and (f) HRTEM images of  $\text{TiO}_{2-x}\text{-C-Sn}$  nanofibers. **The inset in Figure 2d is SAED pattern.**

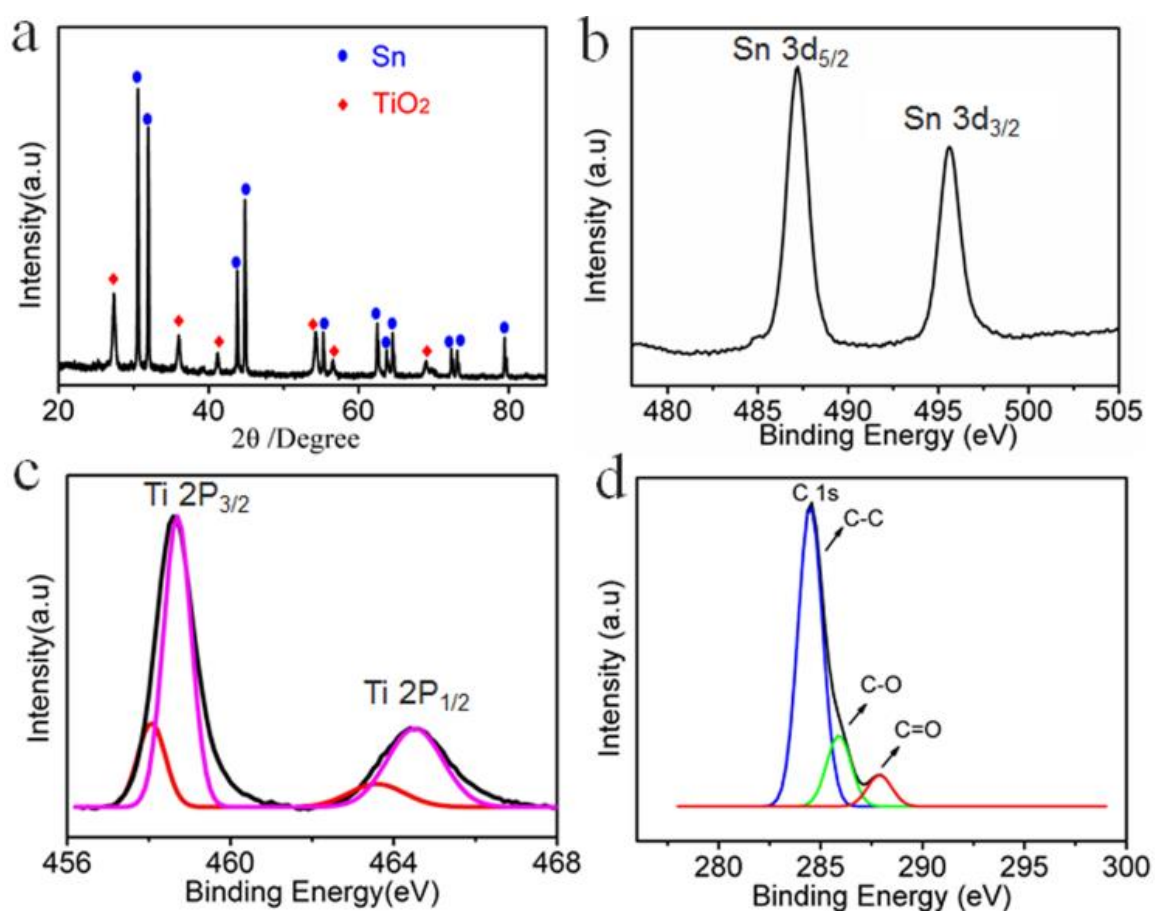


**Figure 3.** Characterization of highly stable porous  $\text{TiO}_{2-x}\text{-C-Sn}$  composite nanofibers. (a) Typical XRD pattern, (b-d) XPS of spectra of the porous  $\text{TiO}_{2-x}\text{-C-Sn}$  composite nanofibers (b) Sn 3d (c) Ti 2p spectrum (d) C 1s spectrum.

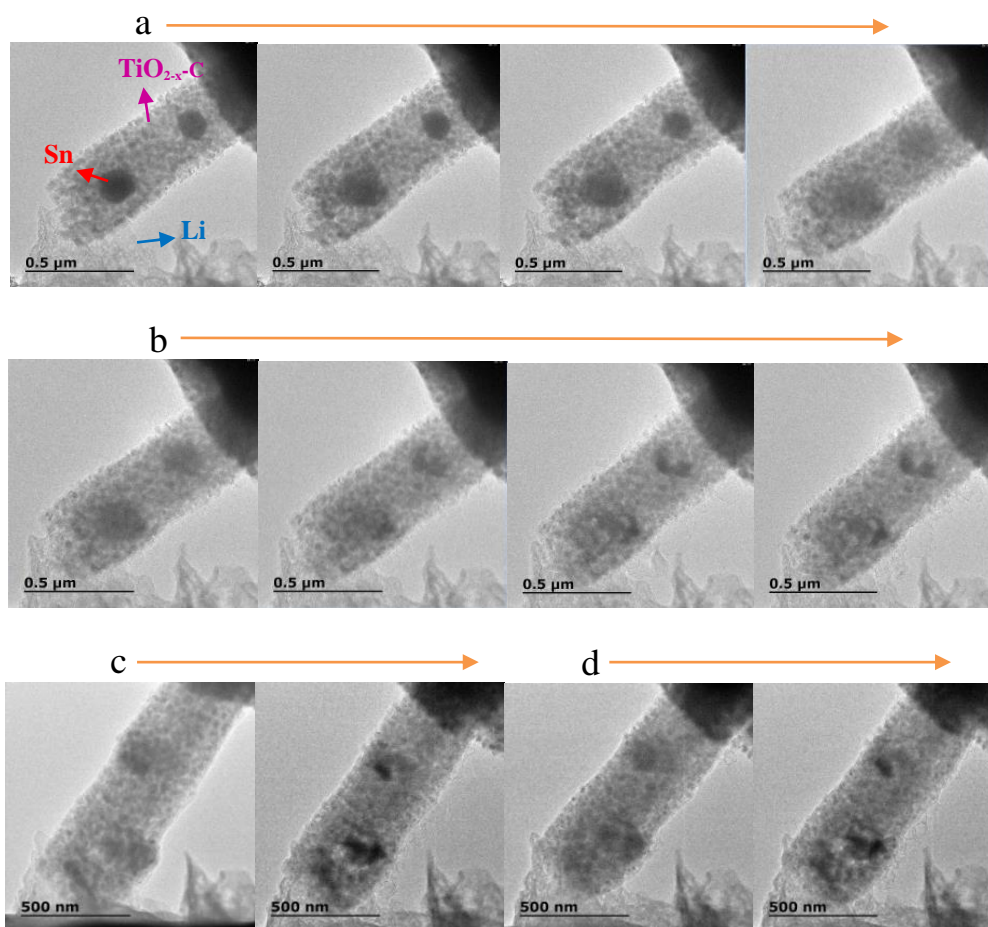


**Figure 4.** Typical morphological evolutions of Sn nanoparticles in the highly stable porous  $\text{TiO}_{2-x}\text{-C}$  nanofiber. (a) The first charging process, (b) the first discharging process, (c) the second charging/discharging steps, and (d) the fifth charging/discharging steps.



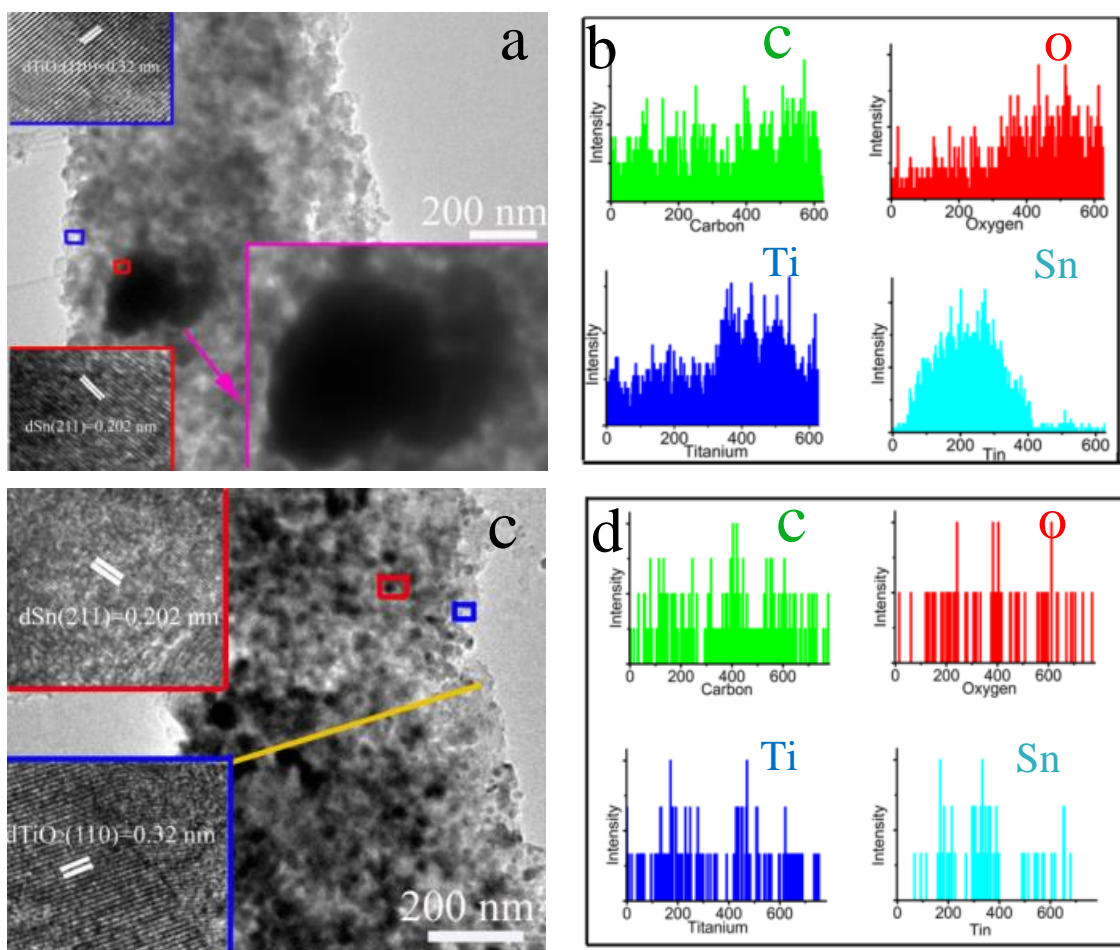


**Figure 5.** TEM and HRTEM images of the highly stable porous  $\text{TiO}_{2-x}\text{-C-Sn}$  composite nanofiber electrode after 1 (a) and 1000 (c) charge-discharge cycles, (b) and (d) corresponding line scanning of (a) and (c).

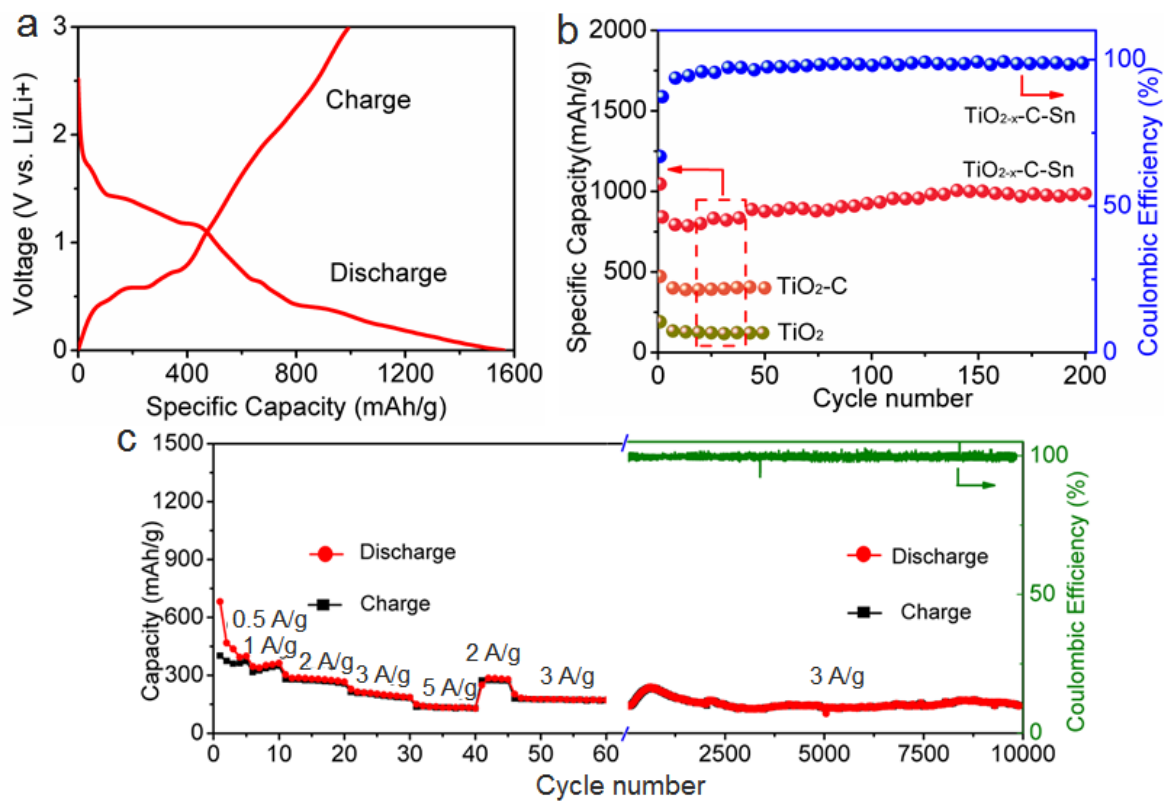


**Figure 6.** Electrochemical performance of the highly stable porous  $\text{TiO}_{2-x}\text{-C-Sn}$  composite nanofiber electrodes. (a) charge-discharge profile, (b) cycling performance of  $\text{TiO}_{2-x}\text{-C-Sn}$ ,  $\text{TiO}_2\text{-C}$  and  $\text{TiO}_2$  nanofibers at the rate of 0.1 A/g, (c) rate and cycling performance of the porous  $\text{TiO}_{2-x}\text{-C-Sn}$  composite nanofibers.

A novel approach induced by lithiation was exploited to insert Sn nanoparticles into the pores of highly stable  $\text{TiO}_{2-x}\text{-C}$  nanofiber substrates that can effectively localize the post-formed smaller Sn nanoparticles and thereby address the problem of structural degradation of Sn anodes and thus show a high capacity of 957 mAh/g after 200 cycles at 0.1 A/g and the longest cycle life of over 10,000 times at 3 A/g while retaining 82.3 % of their capacity.

**Keyword:** lithiation-induced insertion,  $\text{TiO}_{2-x}\text{-C}$ -Sn hybrid nanofibers, *in situ* TEM, electrospinning, lithium ion batteries

Xiaoyan Li,<sup>+</sup> Yuming Chen,<sup>+</sup> Hongtao Wang, Haimin Yao, Haitao Huang, Yiu-Wing Mai, Ning Hu and Limin Zhou\*

### Inserting Sn Nanoparticles into the Pores of $\text{TiO}_{2-x}\text{-C}$ Nanofibers by Lithiation

ToC figure



Copyright WILEY-VCH Verlag GmbH & Co. KGaA, 69469 Weinheim, Germany, 2013.

## Supporting Information

### Inserting Sn Nanoparticles into the Pores of $\text{TiO}_{2-x}\text{-C}$ Nanofibers by Lithiation

Xiaoyan Li,<sup>+</sup> Yuming Chen,<sup>+</sup> Hongtao Wang, Haimin Yao, Haitao Huang, Yiu-Wing Mai, Ning Hu and Limin Zhou\*

<sup>+</sup>The authors contributed equally.

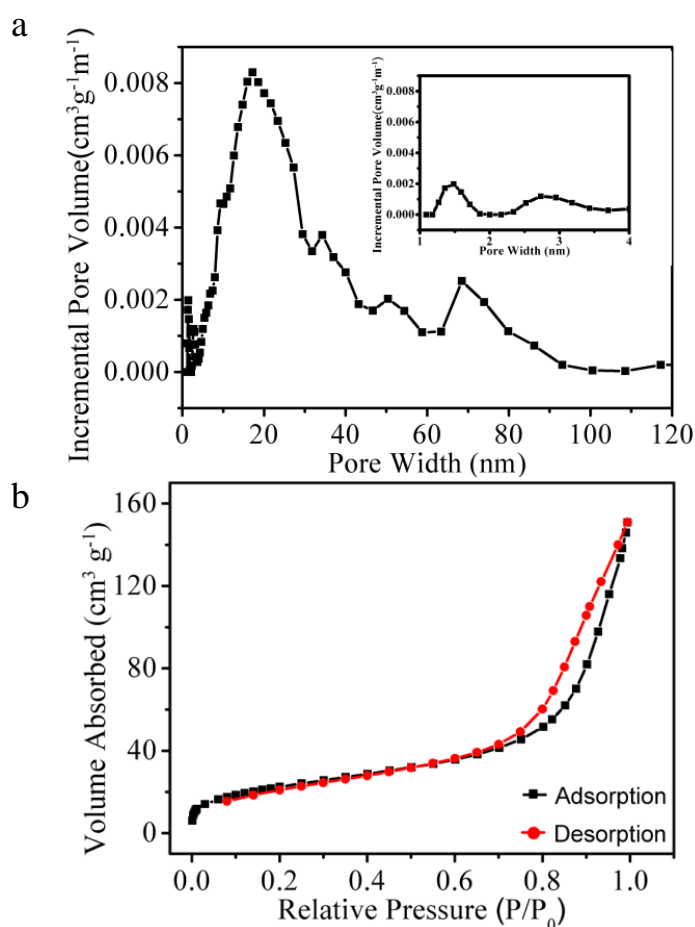


**Figure S1** (a) The pore size distribution and (b) Nitrogen adsorption-desorption isotherm of the highly stable porous  $\text{TiO}_{2-x}\text{-Sn-C}$  nanofibers.

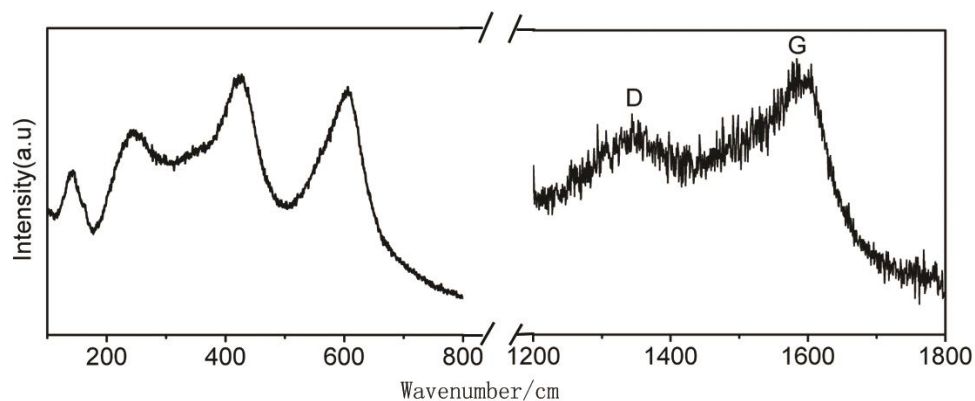


**Figure S2** Raman spectrum of the highly stable porous  $\text{TiO}_{2-x}\text{-C-Sn}$  composite nanofibers. The observed peaks at  $142\text{ cm}^{-1}$ ,  $236\text{ cm}^{-1}$ ,  $424\text{ cm}^{-1}$ , and  $609\text{ cm}^{-1}$  are ascribed to  $\text{B1g}$ , second-order effect,  $\text{Eg}$ , and  $\text{A1g}$  modes, which are characteristic of the rutile  $\text{TiO}_2$ .<sup>1-3</sup> Two additional peaks at  $1350\text{ cm}^{-1}$  and  $1600\text{ cm}^{-1}$  can also be observed in the  $\text{TiO}_{2-x}\text{-C-Sn}$  composite nanofibers, which confirms the presence of carbon in the resulting materials.

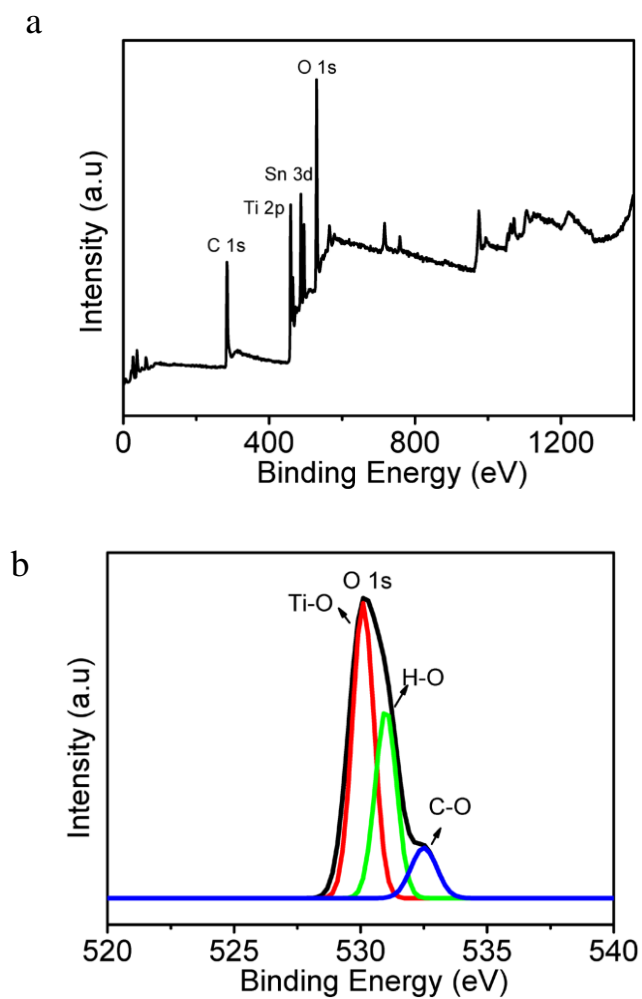


**Figure S3** (a) Typical XPS spectrum of highly stable porous  $\text{TiO}_{2-x}\text{-Sn-C}$  composite nanofibers and (b) O 1s spectrum.

The typical XPS spectrum of the  $\text{TiO}_{2-x}\text{-Sn-C}$  composite nanofibers demonstrates the existence of C, Ti, Sn and O, which is in good agreement with the result of EDS in Figure S4.

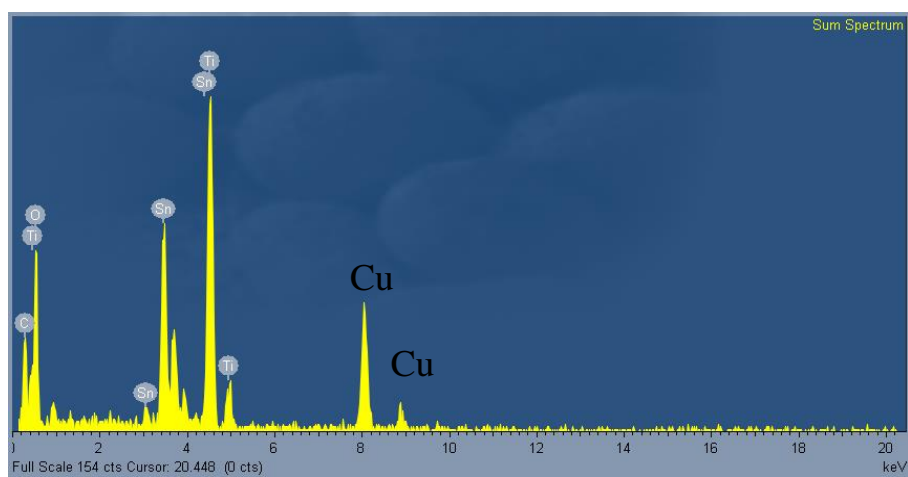


**Figure S4** An EDS spectrum of highly stable porous  $\text{TiO}_{2-x}\text{-Sn-C}$  composite nanofibers.

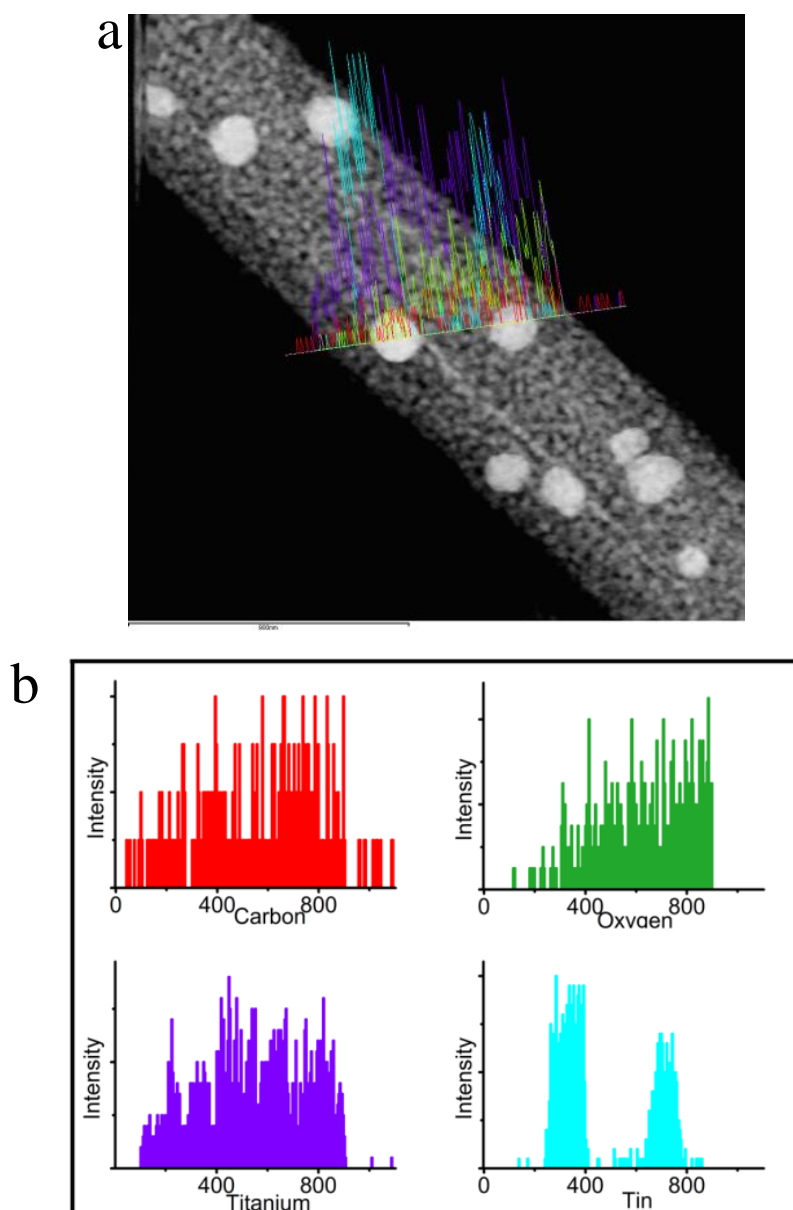


**Figure S5** (a) TEM-BF image and (b) its corresponding EDS elemental line scanning of the  $\text{TiO}_{2-x}\text{-C-Sn}$  composite nanofiber.



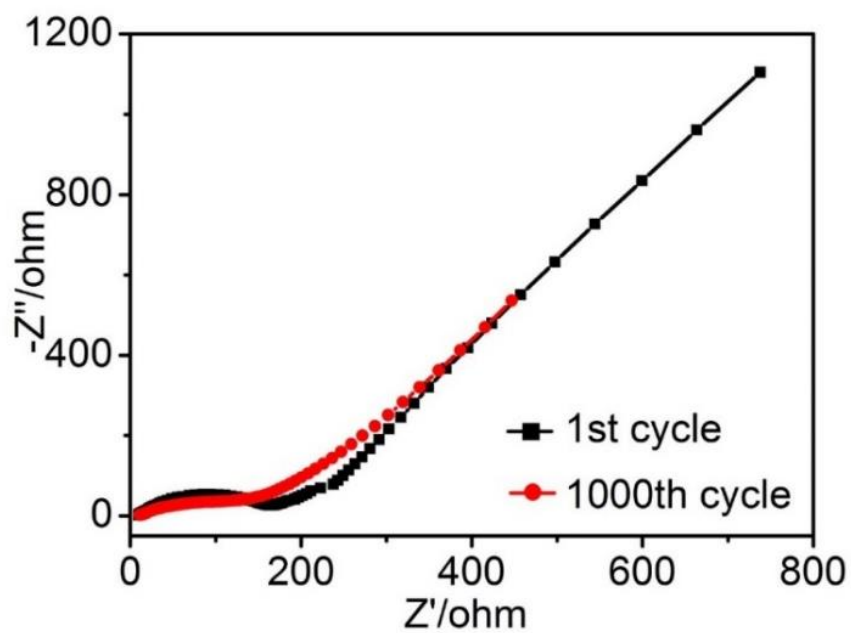


**Figure S6** Nyquist plots of the highly stable porous  $\text{TiO}_{2-x}\text{-C-Sn}$  composite nanofiber electrode after 1 and 1000 cycles in the frequency range from 100 kHz to 10 mHz.

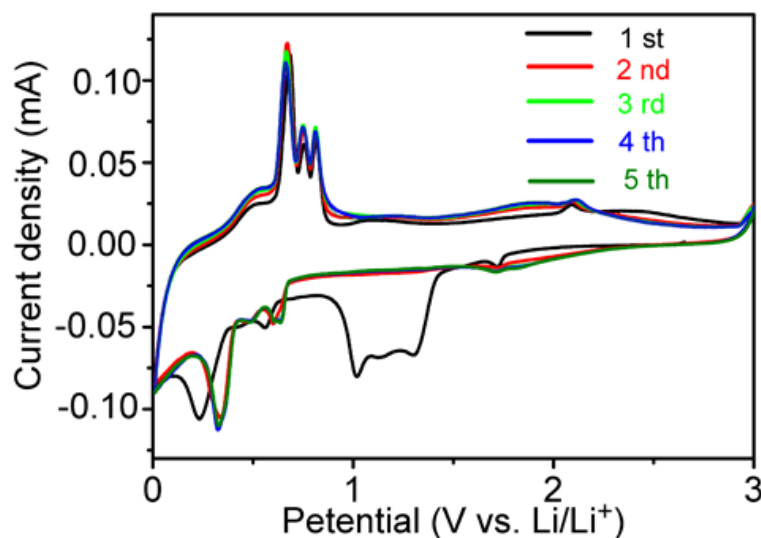


**Figure S7** CV curves of the highly stable porous  $\text{TiO}_{2-x}\text{-C-Sn}$  composite nanofibers. It shows the cyclic voltammograms for the initial five cycles in a potential range of 0 to 3 V vs.  $\text{Li/Li}^+$ .

Notably, a substantial difference can be observed between the first scan and subsequent scans, which is mainly due to the formation of the solid electrolyte interface film.<sup>4-6</sup> In the first scan, the anodic peaks at 0.67, 0.73, and 0.8 V are associated with the dealloying reaction of  $\text{Li}_x\text{Sn}$ , resulting in the formation of Sn. Three cathodic peaks at around 0.3, 0.47, and 0.6 V can be assigned to the lithiation and the formation of  $\text{Li}_x\text{Sn}$  ( $x = 0.4$  to 4.4).<sup>7-10</sup> In addition, two peaks are also observed at 1.7 and 2.1 V, which is ascribed to the insertion and deinsertion of lithium ions into and out of the  $\text{TiO}_2$ .<sup>11</sup> During the subsequent scans, these peaks remain stable, indicating the reversibility of the reaction.

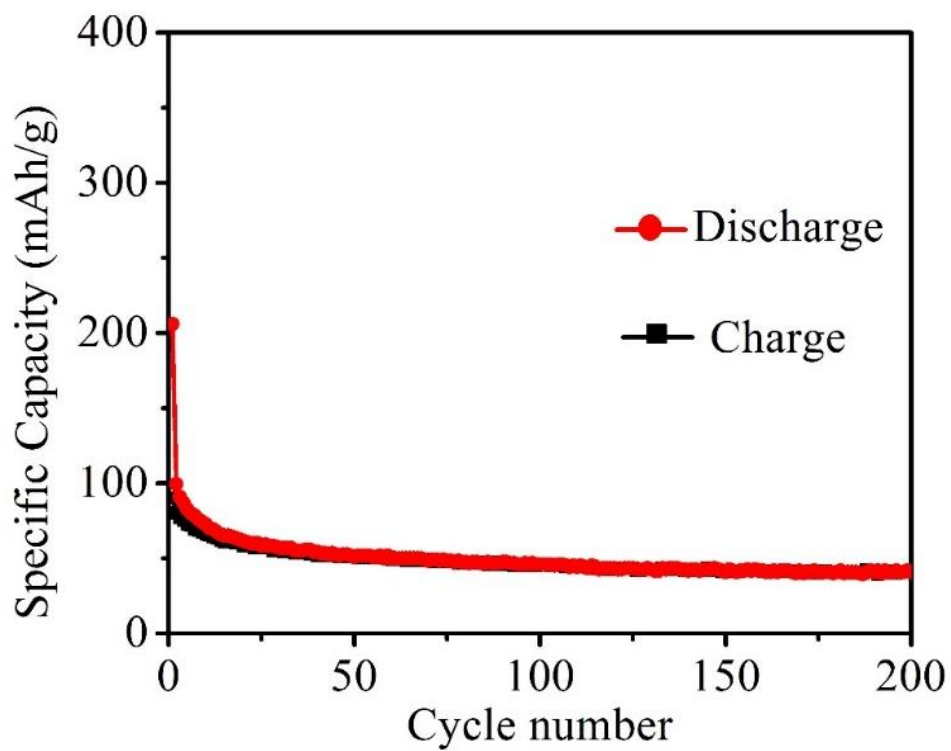


**Figure S8** Cycling performance of TiO<sub>2</sub> at the current density of a current density of 3 A/g.

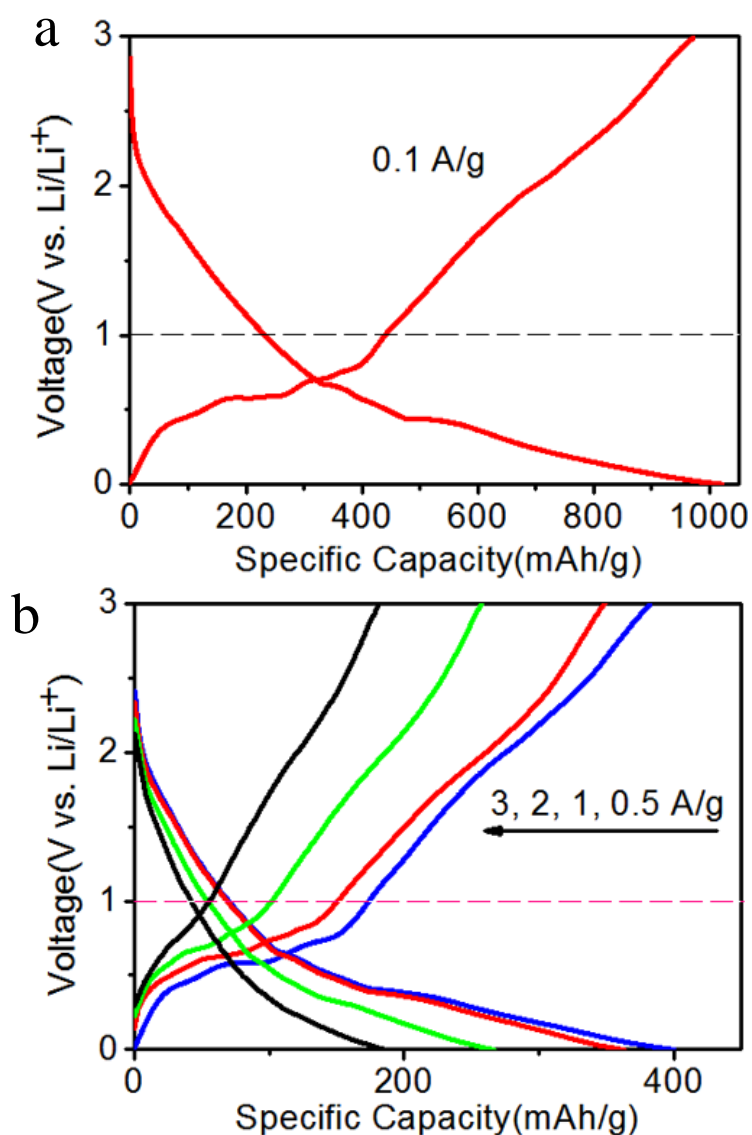


**Figure S9.** Charge-discharge profiles of the porous  $\text{TiO}_{2-x}\text{-C-Sn}$  composite nanofibers (a) after 200 cycles at 0.1 A/g and (b) at different current densities.

It is clear that the plateaus of Sn lithiation and delithiation can be obviously observed after 200 cycles, indicating that the Sn nanomaterials are still well maintained in the  $\text{TiO}_{2-x}\text{-C}$  substrate (Figure S9a). Furthermore, we can see that the capacities between 0-1 V are about 438, 183, 159, 109 and 60 mAh/g at current densities of 0.1, 0.5, 1, 2, and 3 A g<sup>-1</sup>, respectively, which can be mainly due to the contribution of Sn. While the other capacities between 1-3 V would be mainly attributed to the contributions of the  $\text{TiO}_{2-x}\text{-C}$  hybrid and porous structure.

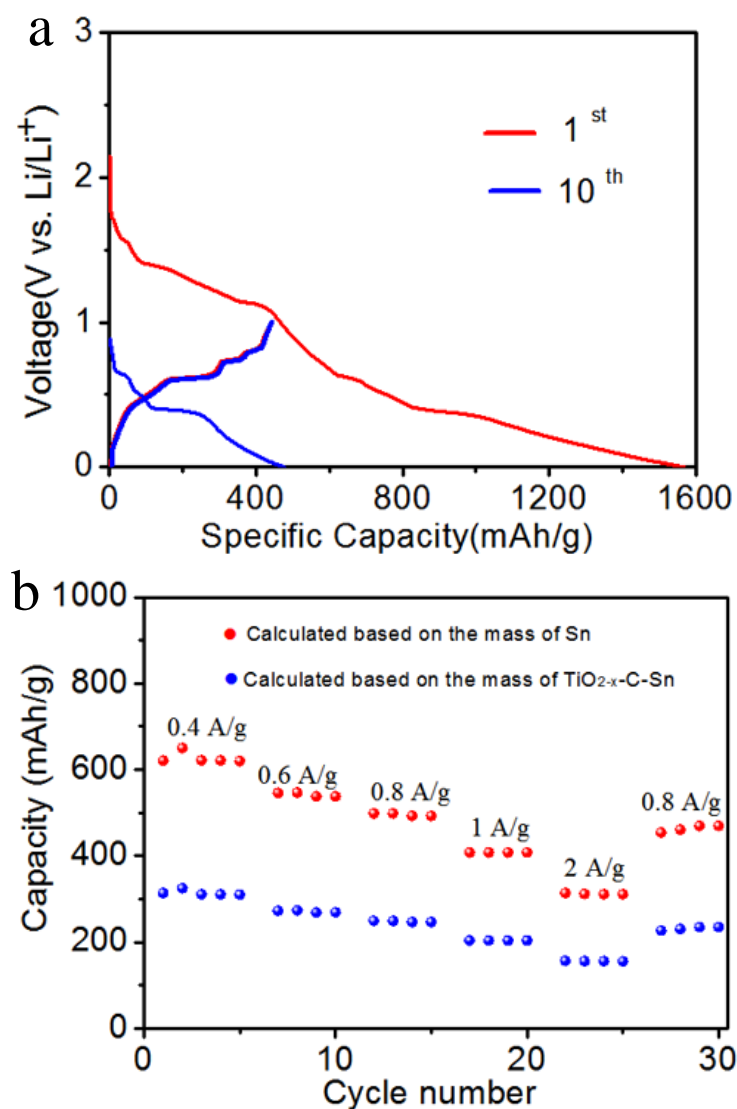


**Figure S10.** (a) The charge-discharge profiles of the porous  $\text{TiO}_{2-x}\text{-C-Sn}$  composite nanofibers at  $0.1\text{A/g}$  based on the mass of the composite and (b) rate performance of the porous  $\text{TiO}_{2-x}\text{-C-Sn}$  composite nanofibers at different current densities in the voltage range of  $0\text{-}1\text{ V}$ .

**Table S1 EDS composite profile of  $\text{TiO}_{2-x}\text{-C-Sn}$  nanofiber**

	C	O	Ti	Sn
Weight /%	8.78	13.55	29.55	48.12
Atomic /%	28.12	32.58	23.72	15.59

**References**

- [1] Y. L. Zhang, C. X. Harris, P. Wallenmeyer, J. Murowchick and X. B. Chen, *J. Phys. Chem. C* **2013**, 117, 24015.
- [2] V. Swamya, B. C. Muddle and Q. Dai, *Appl. Phys. Lett.* **2006**, 89, 163118.
- [3] H. L. Ma, J. Y. Yang, Y. Dai, Y. B. Zhang, B. Lu and G. H. Ma, *Appl. Surf. Sci.* **2007**, 253, 7497.
- [4] Y. Q. Zou and Y. Wang, *ACS Nano* **2011**, 5, 8108.
- [5] D. Deng and J. Y. Lee, *J. Mater. Chem.* **2010**, 20, 8045.
- [6] J. Qin, C. N. He, N. Q. Zhao, Z. Y. Wang, C. S. Shi, E. Z. Liu and J. J. Li, *ACS Nano* **2014**, 8, 1728.
- [7] S. Q. Chen, P. Chen, M. H. Wu, D. Y. Pan and Y. Wang, *Electrochem. Commun.* **2010**, 12, 1302.
- [8] W. M. Zhang, J. S. Hu, Y. G. Guo, S. F. Zheng, L. S. Zhong, W. G. Song and L. J. Wan, *Adv. Mater.* **2008**, 20, 1160.
- [9] Y. Yu, L. Gu, C. B. Zhu, P. A. V. Aken and J. Maier, *J. Am. Chem. Soc.* **2009**, 131, 15984.
- [10] S. Q. Chen, Y. Wang, H.J. Ahn and G. X. Wang, *J. Power Sources* **2012**, 216, 22.
- [11] X. Y. Li, Y. M. Chen, L. M. Zhou, Y. W. Mai and H. T. Huang, *J. Mater. Chem. A* **2014**, 2, 3875.